Stability Robustness Improvement Using Constrained Optimization Techniques

V. Mukhopadhyay*
Joint Institute for Advancement of Flight Sciences, NASA Langley Research Center, Hampton, Virginia

In a multiloop feedback control system, stability margin improvement by singular value shaping can be achieved with a noise adjustment procedure. A direct method for shaping the singular value spectrum using a constrained optimization technique is described. The design algorithm minimizes a standard linear-quadratic Gaussian performance index while it tries to satisfy minimum singular value constraints at the plant input, output, or both. Selected parameters of a stabilizing control law are used as the design variables. The capabilities of this method are demonstrated using a two-input two-output system, which represents a drone aircraft and its lateral attitude control system.

Nomenclature

A, B, C = controller matrices
F, G_u, H = plant matrices
G = plant transfer matrix
g_i = ith constraint
I = identity matrix
$[I + KG]$ = return difference matrix at plant input
$[I + GK]$ = return difference matrix at plant output
J = performance index
j = $\sqrt{-1}$
K = controller transfer matrix
k_n = nth loop gain perturbation in L matrix
L = perturbation matrix
M = order of controller
N_s, N_c, N_o = order of plant, input, and output
N_L = number of feedback loops
N_g = number of constraints
p = element of controller matrices
S = Laplace variable
U = plant input vector
U' = controller output vector
U_{com} = plant input command
V_{com} = controller input command
X_s = plant state vector
X_c = controller state vector
Y = controller input vector
Y' = plant output vector
β = sideslip angle (deg)
δ_1, δ_2 = elevon and rudder deflections (deg)
σ_n = nth singular value
$\bar{\sigma}, \underline{\sigma}$ = maximum and minimum singular value
$\underline{\sigma}_M, \underline{\sigma}_D$ = global minimum and desired singular value
ϕ_n = nth loop phase perturbation in L matrix
$\phi, \dot{\phi}$ = roll angle and rate (deg/s)
$\psi, \dot{\psi}$ = yaw angle and rate (deg/s)
ω = frequency (rad/s)
ω_n = summation frequency point
$tr[\ ]$ = trace of a square matrix
$E[\ ]$ = expected value

Superscripts

$[\ ]^*$ = complex conjugate transpose
$\dot{(\ )}$ = time derivative

Presented as Paper 85-1931 at the AIAA Guidance, Navigation, and Control Conference, Snowmass, CO, Aug. 19-21, 1985; received Sept. 16, 1985; revision received June 6, 1986.

*Associate Research Professor, George Washington University. Associate Fellow AIAA.

Introduction

STABILITY robustness of a multiinput multioutput (MIMO) feedback control system has been characterized by the minimum singular value of the return difference matrix at the plant input or output.[1,2] Stability robustness improvement by singular value shaping can be done using the linear-quadratic-Gaussian (LQG) design technique, which employs so-called fictitious noise or frequency dependent weighting matrices.[3-5] However, the resulting LQG controller is of the same order as the plant. Also, the root-mean-square (RMS) response cannot be used as a measure of response in a constraint function since it contains the effect of fictitious noise. A direct method for shaping the singular value spectrum using a constrained optimization technique was described by Newsom and Mukhopadhyay.[6] There selected parameters of an existing low-order controller were used as design variables to minimize feedback gains while satisfying a given minimum singular-value bound at the plant input. In general, a stability margin improvement at the plant input is accompanied by a stability margin degradation at the plant output and an increase in response and control activity. The present paper describes a design procedure that combines the method of Ref. 6 with the LQG design techniques in order to arrive at a compromise solution using a full-order LQG controller, a reduced-order LQG-type controller,[7] or a low-order conventional controller as design possibilities. The procedure minimizes a standard LQG cost function while attempting to satisfy minimum singular value constraints at the plant input, or output, or at both. Additional constraints such as maximum RMS response, control surface deflection and rate, and dynamic loads on the structure can also be imposed if desired (see Ref. 8 for a gust load alleviation example). The capabilities of the present method are tested using a two-input two-output system which represents a drone aircraft and its lateral attitude-control system.

System Description

Let the multiloop feedback control system shown in Fig. 1 be described by a set of constant coefficient state-space equations, expressed by Eqs. (1-6).

Plant:

$$\dot{X}_s = FX_s + G_u U \tag{1}$$

$$Y' = HX_s \tag{2}$$

Controller:

$$\dot{X}_c = AX_c + BY \tag{3}$$

$$U' = CX_c \tag{4}$$

Interconnection:

$$U = U' + U_{\text{com}} \tag{5}$$

$$Y = Y' + V_{\text{com}} \tag{6}$$

Equation (1) represents an N_sth order plant having N_o output measurements Y' modeled by Eq. (2), and N_c control inputs U. Equations (3) and (4) represent an Mth order feedback controller driven by the output feedback Y. The plant and controller are interconnected by Eqs. (5) and (6), which include external inputs U_{com} and V_{com}. Fictitious white noise processes can be inserted to improve stability margins at these two points.

The plant and the controller transfer matrices in the Laplace domain $G(S)$ and $K(S)$ are defined as

$$Y'(S) = H(IS - F)^{-1}G_u U(S) = G(S)U(S) \tag{7}$$

$$U'(S) = C(IS - A)^{-1}BY(S) = -K(S)Y(S) \tag{8}$$

The argument S will be dropped in the subsequent sections for convenience. For the closed-loop system, one may write

$$\begin{Bmatrix} Y' \\ Y \\ U' \\ U \end{Bmatrix} = \begin{bmatrix} (I+GK)^{-1}G & -(I+GK)^{-1}GK \\ (I+GK)^{-1}G & (I+GK)^{-1} \\ -(I+KG)^{-1}KG & -(I+KG)^{-1}K \\ (I+KG)^{-1} & -(I+KG)^{-1}K \end{bmatrix} \begin{Bmatrix} U_{\text{COM}} \\ V_{\text{COM}} \end{Bmatrix} \tag{9}$$

In the above transfer-matrix relations, the most fundamental matrices are $(I+KG)$ and $(I+GK)$, which govern the stability margins at the plant input and output, denoted by 1 and 2, respectively, in Fig. 1. A brief review of the stability margins and their relations to the matrix singular values follows.

Stability Robustness Review

The stability robustness of multiloop systems and its relation to the singular value of the return difference matrix are discussed in detail in Refs. 4 and 5. Singular values of a matrix A are defined as the positive square roots of the eigenvalues of A^*A. The minimum singular value of the return difference matrix at the plant input $\underline{\sigma}(I+KG)$ and the inverse return difference matrix $\underline{\sigma}(I+(KG)^{-1})$ are measures of stability margin at the plant input in the following sense.

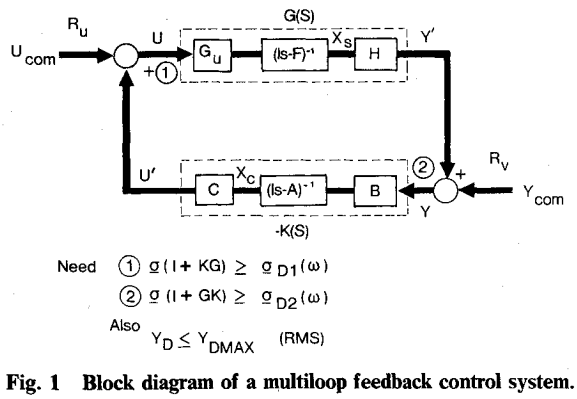

Fig. 1 Block diagram of a multiloop feedback control system.

Let a perturbation matrix L, whose nominal value is unity, be introduced at the plant input, denoted by 1 in Fig. 1. It can be shown[5] that, if the nominal system is stable, then under certain conditions the stability of the perturbed system is guaranteed if

$$\bar{\sigma}(L^{-1} - I) < \underline{\sigma}(I + KG) \tag{10}$$

or

$$\bar{\sigma}(L - I) < \underline{\sigma}\left(I + (KG)^{-1}\right) \tag{11}$$

over all frequencies ($S = j\omega$).

The stability robustness can be expressed in terms of gain and phase margins as follows. Consider a specific L matrix which represents simultaneous gain and phase perturbations k_n and ϕ_n in every loop, namely

$$L = \text{diag}[K_n \exp(j\phi_n)], n = 1,2 \ldots N_L, k_n > 0 \tag{12}$$

At the nominal conditions, $k_n = 1$ and $\phi_n = 0$ for all N_L (i.e., $L = I$). The stability conditions [Eqs. (10) and (11)] can be represented graphically,[1,2] as shown in Fig. 2 by the solid line and dashed line, respectively. From the appropriate minimum singular values, one can obtain the minimum range of variation of the gain k_n and the phase ϕ_n at the plant input within which the system is guaranteed to be stable. Since the inequalities of Eqs. (10) and (11) are conservative conditions, one may choose the larger of the ranges.[1] Also, the actual gain and phase margins can be higher than those obtained from Fig. 2.

If the perturbation is introduced at the plant output denoted by 2 in Fig. 1, then the guaranteed stability conditions are similar to the inequalities of Eqs. (10) and (11), except that all KG terms in the equations and in Fig. 2 are replaced by GK. For a single-input single-output (SISO) system, the terms KG and GK are scalar functions of frequency ω and hence $KG = GK$ for all frequencies. Consequently, the stability

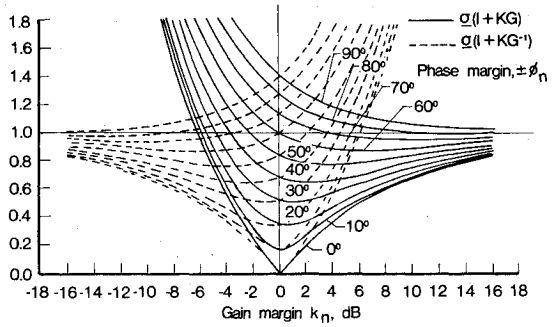

Fig. 2 Universal diagram for gain-phase margin evaluation.

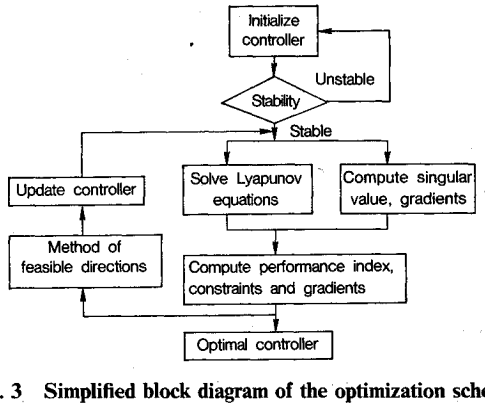

Fig. 3 Simplified block diagram of the optimization scheme.

margins are the same at all points in the loop. However, a MIMO system with a good stability margin at the plant input may have a poor stability margin at the plant output. It is desirable to have good margins at both these locations, and small perturbations at either input or output should not destabilize the system. In Refs. 3–5, a so-called fictitious noise adjustment procedure was described to improve stability margins at the plant input or output. This technique is very useful in arriving at robust LQG controllers for a MIMO feedback control system. The robust controllers obtained by this technique can be improved by the following constrained optimization scheme. A detailed description of this scheme without any constraints may be found in Ref. 7, where full- and reduced-order controller design for a flutter suppression problem was presented.

Optimization Scheme

A simplified block diagram of the optimization scheme is shown in Fig. 3. The basic objective of the control-law synthesis scheme is to find the values of the matrices A, B, and C in Eqs. (3) and (4) which represent a controller or a dynamic compensator for a stable closed-loop system, such that a performance index is minimized and a set of inequality constraints are satisfied. The performance index and constraints are defined next. It is assumed that all external inputs U_{com} and V_{com} are stochastic white-noise processes and all responses are defined by their RMS values. The uncorrelated noise intensity matrices of U_{com} and V_{com} are denoted by R_u and R_v, respectively.

Performance Index

The performance index is in the standard LQG form, defined by a weighted sum of the steady state RMS values of the closed-loop plant and controller output

$$J = E\left[Y'^{T}Q_1Y' + U'^{T}Q_2U'\right] \tag{13}$$

which can be computed by solving a steady-state Lyapunov equation of order $(N_s + M)$. The gradients of the performance index can be computed by solving an adjoint Lyapunov equation of the same order (the details are available in Ref. 7). In order to visualize the role of each noise intensity matrix and weighting matrix in shaping the singular values of different transfer matrices shown in Eq. (9), the performance index in Eq. (13) can be expressed as

$$\begin{aligned} J = \frac{1}{\pi}\int_0^\infty \Big\{ &\sum_i \sigma_i\left[Q_1(I+GK)^{-1}GR_u\right] \\ &+ \sum_i \sigma_i\left[Q_1(I+GK)^{-1}GKR_v\right] \\ &+ \sum_i \sigma_i\left[Q_2(I+KG)^{-1}KGR_u\right] \\ &+ \sum_i \sigma_i\left[Q_2(I+KG)^{-1}KR_v\right]\Big\}\, d\omega \end{aligned} \tag{14}$$

For clarity, the plant disturbance is not included in the formulation shown here. However, it is included in the computations and contributes to the performance index. From Eq. (14), it can be seen that increasing R_u relative to R_v imposes more weight on the first and third terms in Eq. (14), and minimizing J can be interpreted as reducing the general magnitude of $(I + KG)^{-1}KG$ and $(I + GK)^{-1}G$. Since $(I + KG)^{-1}KG = [I + (KG)^{-1}]^{-1}$ and $(I + GK)^{-1}G = G(I + KG)^{-1}$, the minimum magnitudes of $[I + (KG)^{-1}]$ and $(I + KG)$ are increased as a consequence. This increases stability margins at the input. Similarly, increasing R_v relative to R_u imposes more weight on $(I + GK)^{-1}GK$ and $(I + KG)^{-1}K$. By the same argument, minimizing J would increase stability margins at the plant output. Increasing R_v also has the effect of rapid attenuation properties or reduced bandwidth because of the term $(I + KG)^{-1}K$. The weighting matrices Q_1 and Q_2 also play similar roles, as explained in Refs. 3–5.

Constraints

In the constrained minimization approach, the performance index J is minimized by changing the design variables p subject to the inequality constraints

$$g_i(p) \le 0, \qquad i = 1,2 \ldots N_g \tag{15}$$

$g_i(p)$ may represent a constraint on the minimum singular value $\underline{\sigma}(I + KG)$ or $\underline{\sigma}(I + GK)$, or on maximum RMS response.

Constraints on Singular Value

Let us assume that the minimum singular value $\underline{\sigma}(I + KG)$ of a stable system is $\underline{\sigma}_M$, as shown in Fig. 4. It is desired to increase the minimum singular value to a higher level denoted by the line $\underline{\sigma}_D$. Two types of lower bounds are imposed in this paper. The type A denotes a constant $\underline{\sigma}_D$. The type B denotes a frequency dependent $\underline{\sigma}_D(\omega)$, where the singular values are required to attenuate to unity after a specific break frequency. The selection of an achievable $\underline{\sigma}_D(\omega)$ is based on engineering experience and judgment, depending on the control power and response limitations, since control power may be wasted in designing a compensator to satisfy a tight bound with high $\underline{\sigma}_D(\omega)$. Moreover, because of the conservative nature of the singular value measures, inability to obtain such a compensator does not necessarily imply a robustness problem.

The constraint function $g_i(p)$ is basically a cumulative measure of the vertical distance between $\underline{\sigma}_D(\omega)$ and $\underline{\sigma}(I + KG)$

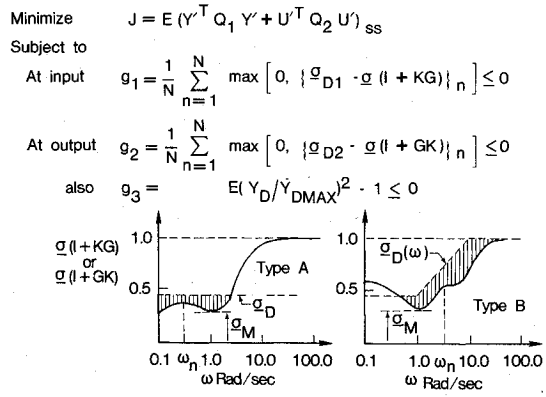

Fig. 4 Geometric description of the cumulative constraints on the minimum singular values $\underline{\sigma}(I + KG)$ and $\underline{\sigma}(I + GK)$.

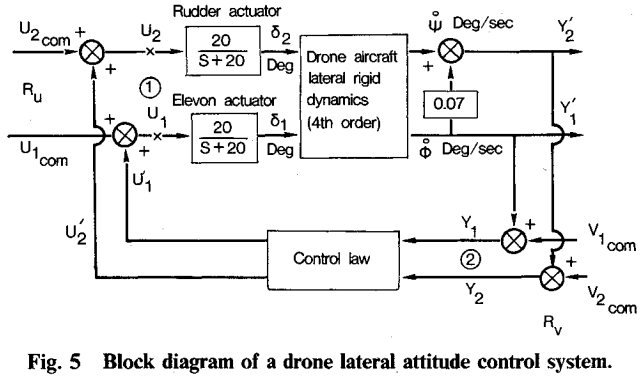

Fig. 5 Block diagram of a drone lateral attitude control system.

or $\underline{\sigma}(I+GK)$, as shown in Fig. 4, and is defined as

$$g_1(p) = \frac{1}{N}\sum_{n=1}^{N}\left[\max\{0,[\underline{\sigma}_D(\omega_n) - \underline{\sigma}(I+KG(j\omega_n,p))]\}\right]^2 \tag{16}$$

$$g_2(p) = \frac{1}{N}\sum_{n=1}^{N}\left[\max\{0,[\underline{\sigma}_D(\omega_n) - \underline{\sigma}(I+GK(j\omega_n,p))]\}\right]^2 \tag{17}$$

The summation is taken over a large number of frequency points ω_n, and the spacing of the frequency points in a frequency range is left to the designer, depending on the specific problem. The objective is to minimize (preferably reduce to zero) the shaded area below the $\underline{\sigma}_D(\omega)$ line by satisfying the inequality constraint of Eq. (15). The expressions for the singular values and their gradients with respect to the design variables are analytically obtained, as described in Ref. 6. Constraints based on Eq. (11) were not used since they are complementary to Eq. (10) and would have added unnecessary computational burden without tangible improvement in results.

Constraint on RMS Response

In the constrained design approach, instead of lumping all the responses in the performance index J, the designer can choose individual responses as a set of inequality constraints

$$g_i(p) = (Y_d/Y_{d\max})_i^2 - 1 \le 0, \qquad i = 2 \text{ or } 3 \ldots N_g \tag{18}$$

where Y_d is the RMS design response, $Y_{d\max}$ is the maximum allowable RMS value, and N_g is the total number of inequality constraints. The response constraints and their gradients with respect to the design variables are analytically obtained by solving a set of Lyapunov equations.

General purpose optimization software[9] which employs the method of usable-feasible directions is used to search for the controller design variables that minimize J subject to $g_i(p) < 0$. The method uses the performance index and constraint gradient information to determine a parameter move direction and a scalar multiplier in the usable-feasible direction in order to satisfy the constraints. During the linear search in the usable-feasible direction, the eigenvalues are monitored to prevent the system from becoming unstable. The method also employs a relaxation technique, where only the constraints close to the $g_i = 0$ boundary are activated in each iteration. It seems to work well when the nominal system does not satisfy the constraints.

Numerical Results

Numerical results are presented for a two-input two-output system that represents a drone aircraft with a lateral attitude control system. A block diagram of the system is shown in Fig. 5. The sixth-order plant state vector is defined as

$$X_s = [\beta\ \dot{\phi}\ \dot{\psi}\ \phi\ \delta_1/20\ \delta_2/20]^T \tag{19}$$

The plant matrices F, G_u, and H, as defined in Eqs. (1) and (2), were presented in Refs. 1, 2, and 6. The eigenvalues of the nominal open-loop system are -0.03701, $0.1889 \pm j1.058$, -3.25, -20, and -20. The unstable complex eigenvalue represents the Dutch-Roll mode. The plant input position 1 is defined at the entry point to the elevon and rudder actuators, denoted by U_1 and U_2 in degrees. The plant output position 2 is defined at the roll rate and yaw rate sensor outputs, denoted by Y_1 and Y_2 in degrees per second.

Design of Full-Order LQG Controller

In this section, the objective is to demonstrate the ability to shape the minimum singular value by adjusting the noise-intensity matrices and to illustrate them with the singular-value plots at the plant input and output, presented in Figs. 6 and 7 for a full-order LQG controller. The noise intensity matrices used in the design are shown beside each plot and in Table 1 and are designated as designs 1 to 6. In all these designs, the weighting matrices are $Q_1 = I$ and $Q_2 = 0.5I$. The full-order LQG controllers are obtained by solving the standard Kalman filter and controller Riccati equation to obtain the filter gain matrix B and C, respectively. The matrix A is given by $A = (F - BH + G_uC)$. In designs 1 to 3, $R_u = I$, and R_v takes the values $100.0I$, I, and $0.01I$, respectively. The resulting singular values are plotted in Fig. 6. In design 1, with the high value of R_v, the minimum $\underline{\sigma}(I+KG) = 0.15$ and $\underline{\sigma}(I+GK) = 0.83$. Most of the stability robustness is at the plant output. The singular values also have rapid attenuation at higher frequencies. In design 2, with $R_v = I$, the minimum $\underline{\sigma}(I+KG) = 0.2$ and $\underline{\sigma}(I+GK) = 0.5$. When R_v is lowered to $0.01I$ in design 3, most of the stability robustness is achieved at the plant input. There is substantial loss of attenuation at higher

Table 1 Summary of design parameters and rms responses

Design no.	Input noise intensity, R_u	Sensor noise intensity, R_v	Order of controller	Design procedure[a]	$\underline{\sigma}_{\min}(I+KG)$	$\underline{\sigma}_{\min}(I+GK)$	RMS Response to unit rms noise at U_1: Side slip, β	Roll rate, $\dot{\phi}$	Yaw rate, $\dot{\psi}$	Elevon defl., δ_1	Rudder defl., δ_2
1	I	100I	6	LQG	0.15	0.83	0.27	2.69	0.59	3.37	0.36
2	I	I	6	LQG	0.20	0.50	0.11	1.68	0.21	3.43	0.25
3	I	0.01I	6	LQG	0.53	0.10	0.11	1.30	0.24	3.26	0.59
4	1000I	I	6	LQG	0.68	0.05	0.09	1.19	0.21	3.14	0.53
5	$\begin{bmatrix}1 & \\ & 100\end{bmatrix}$	$\begin{bmatrix}1 & \\ & 10\end{bmatrix}$	6	LQG	0.33	0.25	0.07	1.24	0.20	3.24	0.45
6	$\begin{bmatrix}0 & \\ & 0\end{bmatrix}$	$\begin{bmatrix}0 & \\ & 0\end{bmatrix}$	6	$O(A)$	0.40	0.38	0.02	1.27	0.13	3.31	0.22
7	$\begin{bmatrix}0 & \\ & 0\end{bmatrix}$	$\begin{bmatrix}0 & \\ & 0\end{bmatrix}$	3	T	0.17	0.10	0.16	1.56	0.19	3.26	0.36
8	$\begin{bmatrix}0 & \\ & 0\end{bmatrix}$	$\begin{bmatrix}0 & \\ & 0\end{bmatrix}$	3	$O(A)$	0.22	0.40	0.03	1.48	0.14	3.59	0.71
9	$\begin{bmatrix}0 & \\ & 0\end{bmatrix}$	$\begin{bmatrix}0 & \\ & 0\end{bmatrix}$	3	$O(B)$	0.26	0.22	0.08	1.46	0.14	3.25	0.12

[a] $O(A)$ = Optimization (type A constraint). $O(B)$ = Optimization (type B constraint). T = Truncation of design 6.

frequencies. Note that the ratio of R_u to R_v is the main factor in these noise adjustment procedures. In design 4, shown in Fig. 7, the stability margin at the input is increased further using $R_u = 1000I$ and $R_v = I$. The effect of unequal noise intensity in each loop is investigated in design 5, which uses $R_u = \text{diag}[1\ 100]$ and $R_v = \text{diag}[1\ 10]$, imposing more uncertainty in the rudder channel. The minimum singular value plot shown in Fig. 7 indicates that the minimum $\underline{\sigma}(I + KG)$ is 0.33 and the minimum $\underline{\sigma}(I + GK)$ is 0.25, and that both have good high frequency attenuation. This design is used as the starting point for testing the present constrained optimization design procedure to improve stability robustness at both the plant input and output. In these designs, the weighting matrices Q_1 and Q_2 are the same as before. The noise intensity matrices R_u and R_v are set to zero. The system only contains a unit RMS white noise input at the elevon actuator. All the elements of the matrices B and C are chosen as design variables. The minimum desired singular value $\underline{\sigma}_D = 0.45$ is chosen to constrain $\underline{\sigma}(I + KG)$ and $\underline{\sigma}(I + GK)$ at the plant input and output, respectively. A type 'A' constraint is used in designs 6 and 8 and a Type 'B' constraint is used in design 9. Figure 4 shows the exact shape of the constraint $\underline{\sigma}_D(\omega)$ imposed on the singular values $\underline{\sigma}(I + KG)$ and $\underline{\sigma}(I + GK)$. The frequency ranges from 0.1 to 100 rad/s, beyond which both KG and GK attenuate to zero for all designs. All high-frequency uncertainties are assumed to be above 100 rad/s. In the cumulative constraints of Eqs. (16) and (17), the frequency points are uniformly chosen as 50 divisions per decade. In all the design cases, the optimization cycle was stopped after five iterations, since more iterations usually resulted only in marginal improvements.

In design 6, the full-order controller obtained in design 5 was optimized. After five iterations, the minimum singular values are reshaped, as shown in Fig. 7. The minimum values of $\underline{\sigma}(I + KG)$ and $\underline{\sigma}(I + GK)$ are increased from 0.33 and 0.25 to 0.4 and 0.38, respectively. Thus the present constrained optimization procedure is able to improve stability robustness at both input and output. However, the improvement is at the cost of some loss of high frequency attenuation at the input. The open- and closed-loop eigenvalues are shown in Table 2. The eigenvalues and transient response plots (not presented here) indicate adequate damping of the Dutch roll, heading, and roll modes for a drone aircraft.

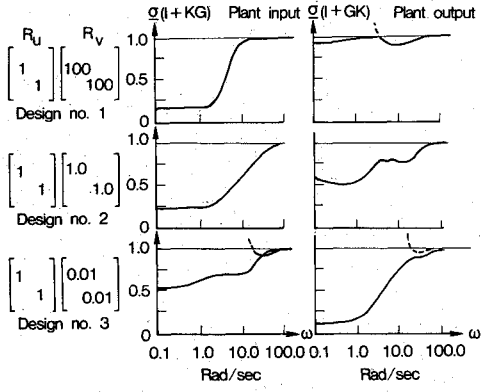

Fig. 6 Singular value shaping by noise adjustment (full order controller).

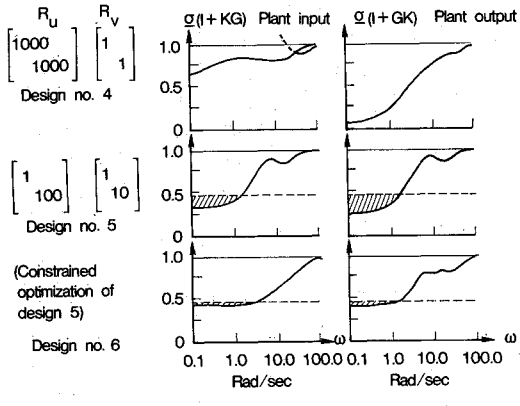

Fig. 7 Singular value shaping by noise adjustment and constrained optimization (full order controller).

Design of Reduced-Order Controller

The next three designs, designated as designs 7 to 9 in Table 1 represent results of an attempt to obtain reduced-order controllers, starting from design 6 using truncation and then a constrained optimization technique. First, a third-order controller is obtained from controller 6, retaining only the second, third, and sixth states, which correspond to the roll rate, yaw rate, and rudder actuator states. In Table 1, this is designated at design 7. The fact that such a truncated controller can stabilize the system is a manifestation of the stability robustness of design 6. The corresponding minimum singular value plots of $(I + KG)$ and $(I + GK)$ are shown in Fig. 8. The minimum values of $\underline{\sigma}(I + KG)$ and $\underline{\sigma}(I + GK)$ are 0.17 and 0.1, respectively. To improve its stability robustness, the pres-

Table 2 The plant eigenvalues for open- and closed-loop system

Mode	Open-loop	Closed-loop	
		Design 6	Design 9
Spiral	−0.03701	−0.04662	−0.202
Dutch roll	$0.1889 \pm j1.058$	$-1.1887 \pm j1.752$	$-0.835 \pm j1.203$
Roll	−3.25	−3.56	−7.68
Actuator	−20	−19.98	$-20.06 \pm j1.714$
Actuator	−20	−20.474	

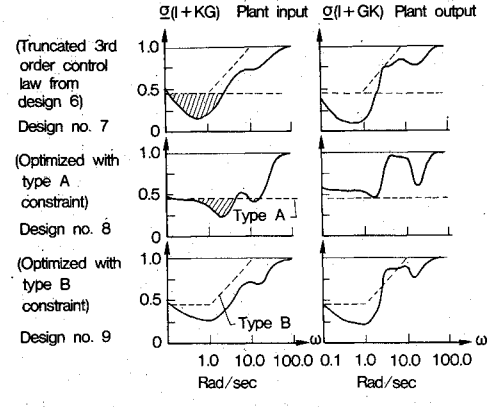

Fig. 8 Singular value shaping by constrained optimization (third order controller).

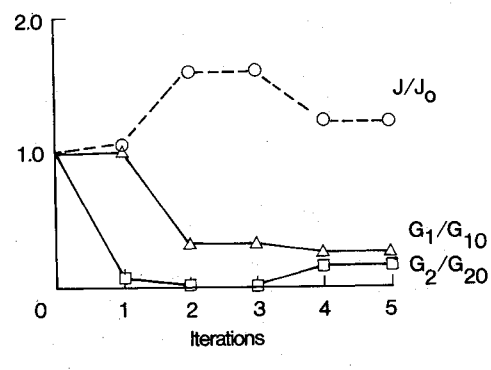

Fig. 9 Normalized performance index and constraints variation with iteration (design 6).

ent constrained optimization procedure is applied with Type '*A*' and Type '*B*' constraints. The results are designated as designs 8 and 9 in Table 1. The B and C matrices in Eqs. (3) and (4) are the design variables. After five iterations, the minimum singular values $\underline{\sigma}(I+KG)$ and $\underline{\sigma}(I+GK)$ are reshaped, as shown in Fig. 8. This represents a moderate improvement at the plant input and output. The improvement is at the cost of some loss of high-frequency attenuation.

The numerical examples indicate that an increase in the minimum singular value at the plant input is always accompanied by a decrease in the minimum singular value at the plant output and vice versa. Using the present procedure, the minimum singular values can be increased at both plant input and output, but only to a limited extent. This is due to the intrinsic relations between $\underline{\sigma}(I+KG)$ and $\underline{\sigma}(I+GK)$, as discussed in Refs. 4 and 5.

RMS Response

The RMS response of the system for a unit RMS noise at the plant input U_1 was computed using covariance analysis. The RMS side slip β, roll rate $\dot{\phi}$, yaw rate $\dot{\psi}$, and elevon and rudder deflections δ_1, δ_2, are presented in Table 1. The general trend in designs 1 to 6 is a progressive reduction of the RMS responses of β, $\dot{\phi}$, and $\dot{\psi}$, while δ_1 and δ_2 remain more or less the same. Designs 6 and 8 have very low side-slip response. In designs 7 to 9, the controller order reduction through truncation and reoptimization did not result in a significant increase in responses when compared to design 6. The design software has the provision of treating each of these responses as individual constraints instead of lumping them in the performance index. The variation of the normalized performance index and constraints on singular values at the plant input and output is shown in Fig. 9 for design 6. The RMS responses and weighting matrices indicate that U and Y contribute roughly equally to the performance index J. After the first iteration, g_2 is nearly satisfied with a slight increase in J. After the second iteration, g_1 is also reduced at the cost of increased J. During iteration four, the algorithm attempts to minimize the performance index J by slightly violating the second constraint g_2 to reach a compromised solution. The convergence patterns for designs 8 and 9 are similar.

Conclusions

This paper describes a design methodology that uses constrained optimization techniques to improve the stability margins of a multiloop system at both the plant input and output, while minimizing a standard linear-quadratic-Gaussian performance index. The capabilities of the method are demonstrated using a two-input two-output system which represents a drone aircraft and its lateral attitude control system. Both full-order and reduced-order controllers were designed for stability robustness at both input and output. The examples show that the constrained optimization procedure can be used in conjunction with the noise adjustment procedure to improve the stability margin at the plant input, or plant output, or, to a limited extent, at both. Additional studies are necessary to simultaneously improve stability margins and shape the transient response.

Acknowledgment

This work was supported by NASA grant NAG1-199.

References

[1]Ly, U.-L., "Robustness Analysis of a Multiloop Flight Control System," AIAA Paper 83-2189, Aug. 1983.

[2]Mukhopadhyay, V. and Newsom, J.R., "A Multiloop System Stability Margin Study Using Matrix Singular Values," *Journal of Guidance, Control, and Dynamics*, Vol. 7, Sept.-Oct. 1984, pp. 582-587.

[3]Doyle, J. C. and Stein, G., "Robustness with Observers," *IEEE Transactions on Automatic Control*, Vol. AC-24, April 1979, pp. 607-611.

[4]Safonov, M.G., Laub, A.J., and Hartmann, G.L., "Feedback Properties of Multivariable Systems: The Role and Use of the Return Difference Matrix," *IEEE Transactions on Automatic Control*, Vol. AC-26, Feb. 1981, pp. 47-65.

[5]Lehtomaki, A.N., Sandell, N.R. Jr., and Athans, M., "Robustness Results in Linear Quadratic Gaussian Based Multivariable Control Design," *IEEE Transactions on Automatic Control*, Vol. AC-26, No. 1, Feb. 1981, pp. 75-92.

[6]Newsom, J.R. and Mukhopadhyay, V., "The Use of Singular Value Gradients and Optimization Techniques to Design Robust Controller for Multiloop Systems," AIAA Paper 83-2191, Aug. 1983.

[7]Mukhopadhyay, V., Newsom, J.R., and Abel, I., "A Method for Obtaining Reduced Order Control Laws for High Order Systems Using Optimization Techniques," NASA TP-1876, Aug. 1981.

[8]Newsom, J.R. and Mukhopadhyay, V., "Application of Constrained Optimization to Active Control of Aeroelastic Response," NASA TM-83150, June 1981.

[9]Vanderplatts, G.D., "CONMIN—A Fortran Program for Constraint Function Minimization. User Manual," NASA TM-X-62282, Aug. 1973.